

Topology and Interactions in a Frustrated Slab: Tuning from Weyl Semimetals to $\mathcal{C} > 1$ Fractional Chern Insulators

E. J. Bergholtz,¹ Zhao Liu,² M. Trescher,¹ R. Moessner,³ and M. Udagawa⁴

¹*Dahlem Center for Complex Quantum Systems and Institut für Theoretische Physik, Freie Universität Berlin, Arnimallee 14, 14195 Berlin, Germany*

²*Department of Electrical Engineering, Princeton University, Princeton, New Jersey 08544, USA*

³*Max-Planck-Institut für Physik komplexer Systeme, Nöthnitzer Straße 38, D-01187 Dresden, Germany*

⁴*Department of Applied Physics, University of Tokyo, Hongo 7-3-1, Bunkyo-ku, Tokyo 113-8656, Japan*

(Received 28 August 2014; published 8 January 2015)

We show that, quite generically, a [111] slab of spin-orbit coupled pyrochlore lattice exhibits surface states whose constant energy curves take the shape of Fermi arcs, localized to different surfaces depending on their quasimomentum. Remarkably, these persist independently of the existence of Weyl points in the bulk. Considering interacting electrons in slabs of finite thickness, we find a plethora of known fractional Chern insulating phases, to which we add the discovery of a new higher Chern number state which is likely a generalization of the Moore-Read fermionic fractional quantum Hall state. By contrast, in the three-dimensional limit, we argue for the absence of gapped states of the flat surface band due to a topologically protected coupling of the surface to gapless states in the bulk. We comment on generalizations as well as experimental perspectives in thin slabs of pyrochlore iridates.

DOI: 10.1103/PhysRevLett.114.016806

PACS numbers: 73.43.Cd, 71.10.Fd, 73.21.Ac

Introduction.—The prediction [1–5] and subsequent experimental observation [6,7] of topological insulators has fundamentally revolutionized the understanding of electronic states of matter during the past decade [8–10]. New frontiers in this field include gapless topological phases such as three-dimensional Weyl semimetals [11–15] exhibiting exotic Fermi arc surface states [13,15–17], interaction effects on the gapless surface of topological insulators [18–22], and strongly correlated phases akin to fractional quantum Hall states in two-dimensional (2D) lattices (see Refs. [23,24] and references therein). Drawing additional inspiration from the rapid development of growth techniques in fabricating high quality slabs, films, or interfaces of oxide materials [25], this work provides intriguing connections between these seemingly disparate frontiers.

The materials pursuit for Weyl semimetals and their relatives is rapidly broadening [26–29], with spin-orbit coupled pyrochlore iridates, such as $\text{Y}_2\text{Ir}_2\text{O}_7$ [13,30–32] being particularly promising compounds—as these are favorably grown or cleaved in the [111] direction, and given their predicted rich variety of strongly correlated phases [33,34], we here study the surface bands of pyrochlore [111] slabs, where the system can be seen as a layered structure of alternating kagome and triangular layers [30] (Fig. 1).

Our work uncovers an intriguing dichotomy between bulk and surface states which allows us to establish connections between apparently disparate topological phenomena. While the bulk band structure changes drastically as a function of the inter-layer tunneling strength t_\perp —including the (dis)appearance of the Weyl semimetal—the surface states, which involve only the kagome layers,

remain unchanged on account of their essentially geometrical origin. Most saliently, in the two distinct regimes of N weakly coupled kagome layers, each with unit Chern number, at small t_\perp , and the genuinely three-dimensional Weyl semimetal at large t_\perp , identical surface states carrying Chern number $\mathcal{C} = N$ are localized at opposite surfaces depending on their momentum. Constant energy contours in reciprocal space are Fermi arcs, which thus exist also in the absence of Weyl nodes in the bulk.

Upon adding interactions to a partially filled surface band—even when these are made very flat by tuning hopping parameters—we argue that interactions do not open a gap for thick slabs, due to a leakage into the bulk along “soft” lines related to projections of remnant Weyl nodes. However, in thin slabs we find a plethora of possible fractionalized phases, some of which were discovered earlier [33,34] with the implicit assumption of subcritical interlayer tunneling. Most prominently, we provide evidence for a first non-Abelian fermionic fractional Chern insulator (FCI) in a $\mathcal{C} > 1$ band, namely a $\mathcal{C} = 2$ generalization of the Moore-Read quantum Hall phase [35]. Our work thus gives a unifying and fresh perspective on the intriguing combination of fractionalization and topological surface localization impossible in strictly two-dimensional systems.

Setup.—Our tight binding model on N kagome layers, \mathcal{K}_m , alternating with $N - 1$ triangular layers, \mathcal{T}_m [30] (Fig. 1), considers spinless, spin-orbit coupled, fermions with interlayer hopping amplitude t_\perp and kagome layer (next) nearest hopping amplitudes $t_1 \pm i\lambda_1$ ($t_2 \pm i\lambda_2$), where the $-(+)$ sign applies for (anti-)clockwise hopping with respect to the hexagon on which it takes place.

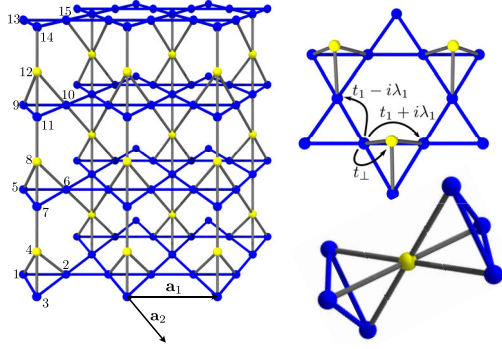


FIG. 1 (color online). The pyrochlore slab. The left panel shows the [111] pyrochlore slab with $N = 4$ kagome layers (dark blue) separated by (yellow) sites of $N - 1 = 3$ triangular layers. A practical labeling of the $4N - 1 = 15$ sites in the unit cell and the basis vectors, $\mathbf{a}_1, \mathbf{a}_2$, of the Bravais lattice are also indicated. The top right panel indicates the considered nearest-neighbor processes. The lower right panel shows the local environment of a triangular (yellow) site for which the local constraint of destructive interference directly leads to the surface states (1).

Time-reversal symmetry is absent, e.g., due to an orbital field or spontaneous ferromagnetism.

Band structure and surface wave functions.— Independently of the form of the Bloch states of a single kagome layer, three bands of the N -layer system are exactly described by

$$|\psi^i(\mathbf{k})\rangle = \mathcal{N}(\mathbf{k}) \sum_{m=1}^N (r(\mathbf{k}))^m |\phi^i(\mathbf{k})\rangle_m, \quad (1)$$

where $|\phi^i(\mathbf{k})\rangle_m$, $i = 1, 2, 3$ are the single layer Bloch states localized to \mathcal{K}_m and $\mathcal{N}(\mathbf{k})$ ensures proper normalization. The coefficients $r(\mathbf{k})$ are determined by demanding that the amplitudes for hopping to the triangular layers vanish by interfering destructively (Fig. 1): $r(\mathbf{k}) = -[\phi_1^i(\mathbf{k}) + \phi_2^i(\mathbf{k}) + \phi_3^i(\mathbf{k})] / [e^{-ik_2}\phi_1^i(\mathbf{k}) + e^{i(k_1-k_2)}\phi_2^i(\mathbf{k}) + \phi_3^i(\mathbf{k})]$, where $\phi_n^i(\mathbf{k})$, $n \leq 3$, are the components of the Bloch spinor for the pertinent state $|\phi^i(\mathbf{k})\rangle$ in a single kagome layer, and $k_{1,2} = \mathbf{k} \cdot \mathbf{a}_{1,2}$. While $\phi_n^i(\mathbf{k})$, $n \leq 3$, can be analytically obtained by diagonalizing 3×3 Hermitian matrices, the full Bloch spinor is fully known via $\psi_{4m}^i(\mathbf{k}) = 0$, $\psi_{n+4(m-1)}^i(\mathbf{k}) = \mathcal{N}(\mathbf{k})[r(\mathbf{k})]^m \phi_n^i(\mathbf{k})$ for all \mathbf{k}, n, m , with $E(\mathbf{k})$ of the states (1) equal to those of the single layer case.

Let us emphasize that, first, the states on the slab are exponentially localized to either the top or bottom layers, except in high symmetry cases where $|r(\mathbf{k})| = 1$. And second, if periodic boundary conditions are applied also in the [111] direction, there are *no* generic eigenstates of the form (1), underscoring their surface nature.

In the following, we consider the case of single layer kagome bands carrying nonzero Chern number [36–38], say $C = 1$. Then, the multilayer state (1) has Chern number N :

$$|\psi^{C=N}(\mathbf{k})\rangle = \mathcal{N}(\mathbf{k}) \sum_{m=1}^N (r(\mathbf{k}))^m |\phi^{C=1}(\mathbf{k})\rangle_m, \quad (2)$$

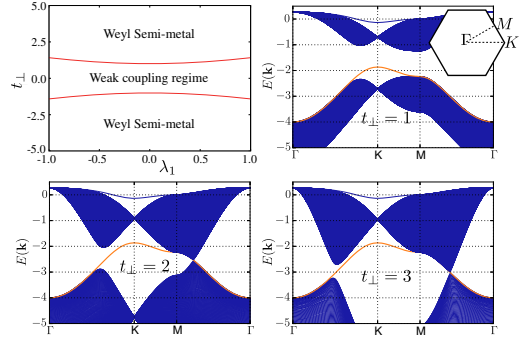


FIG. 2 (color online). Weakly coupled Chern insulators versus Weyl semimetals. As t_{\perp} is increased there is a transition from a weakly coupled regime to a distinct phase where Weyl nodes occur on the line connecting Γ and M . In the top left panel we show the phase diagram in the case of nearest-neighbor hopping only (we set $t_1 = -1$ throughout) [39]. The other panels show example band structures with fixed $\lambda_1 = 0.5$ and varying $t_{\perp} = 1, 2, 3$ for a slab with $N = 300$ kagome layers along the crucial $\Gamma - K - M - \Gamma$ path through the projected 2D Brillouin zone (BZ) (cf. top right inset). Note that, remarkably, the band highlighted in orange corresponding to the surface states (2), is independent of t_{\perp} .

where $|\phi^{C=1}(\mathbf{k})\rangle_m$ is the state localized to \mathcal{K}_m . The states (2) play a prominent role in this work, and their corresponding energies are highlighted in bold orange throughout this work (not shown are the two related states with $C = 0, -N$).

Figure 2 illustrates the finite t_{\perp} transition between weakly coupled Chern insulators and the Weyl semimetal regime with linear band touching points described by

$$H_{\text{Weyl}} = \sum_i v_i \sigma_i k_i + E_0(\mathbf{k}) \mathbb{1}, \quad (3)$$

where σ_i are Pauli matrices and $\mathbb{1}$ is the identity matrix. Precisely at the transition, the valence and conduction bands exhibit a twofold degenerate touching at the M points, which split into three pairs of (nondegenerate) Weyl cones that travel towards the Γ point where they meet as $t_{\perp} \rightarrow \infty$. Remarkably, the states (2) are entirely independent of the value of t_{\perp} ; in each case they describe states localized to the surfaces perpendicular to the [111] cleavage, cut, or growth direction, while at the same time their interpretation fundamentally changes. Note also that the dispersion of the states (2) always traverses the Weyl point.

At fixed chemical potential, which may be fixed at the Weyl node due to stoichiometric considerations, the states (2) precisely describe Fermi arcs. In Fig. 3 we illustrate the momentum dependence of the surface localization of the states (2). Most saliently, we find that the penetration depth diverges along the lines connecting Γ and M . Crossing these lines, the localization changes between the bottom and top surfaces, which is the hallmark behavior of Fermi arcs. More specifically, a typical Fermi “circle” splits into six Fermi arcs which switch between top and

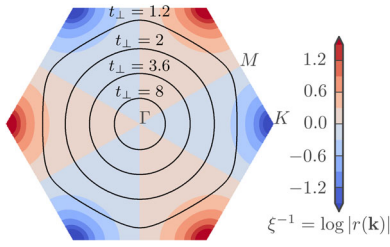


FIG. 3 (color online). Surface state structure and Fermi arcs. The color scale indicates the inverse penetration depth, $\xi^{-1}(\mathbf{k}) = \log(|r(\mathbf{k})|)$ of the surface states throughout the 2D BZ for the same parameters, $t_{\perp} = -1, \lambda_1 = 0.5$, used in Fig. 2. The black lines illustrate Fermi arcs for a chemical potential set at the Weyl node for a few t_{\perp} values. When $\xi^{-1}(\mathbf{k})$ changes sign, the localization changes between top (red) to bottom (blue) surfaces, hence splitting the Fermi circle into six spatially disjoint arcs.

bottom surface six times, whenever the Fermi circle crosses a Γ - M line (cf. Fig. 3).

In Fig. 4 we go on to show how the state (2) can smoothly be transformed into a band which is essentially dispersionless, yet being tightly attached to bulk bands (for thick slabs). It is important to note that also the latter regime is described by a Weyl Hamiltonian (3) with a suitable choice of $E_0(\mathbf{k})$; the essential point is that the topology is unchanged as long as the band touching is

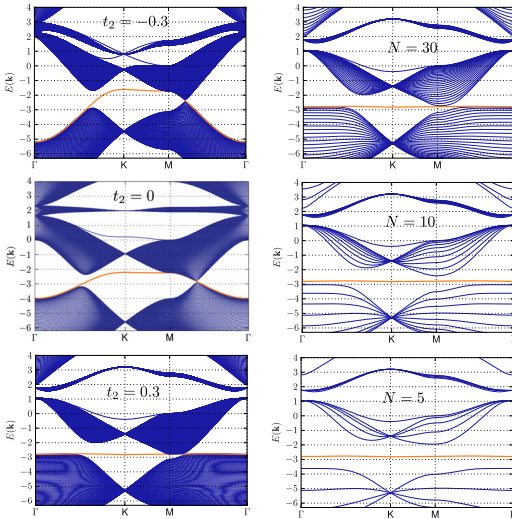


FIG. 4 (color online). From Weyl nodes to flat surface bands. For $t_1 = -1, \lambda_1 = 0.3, \lambda_2 = 0.2, t_{\perp} = 2.0$, we plot the energy dispersion for various N and t_2 on the path Γ - K - M - Γ through the BZ. In the left panel we set the number of kagome layers to $N = 100$ while varying t_2 . For $t_2 = -0.3$ (top) there is a clearly visible Weyl node on the line connecting M and Γ . For $t_2 = 0$ the node is skewed and at $t_2 = 0.3$ it is essentially flattened while the surface band (bold orange) remains at almost fixed energy throughout the entire BZ. In the right panel we fix $t_2 = 0.3$ and reduce the number of layers, $N = 30, 10, 5$, from top to bottom, and a sizable finite size gap quickly opens throughout the entire BZ. The band highlighted in bold orange is that of (2), carrying Chern number $C = N$.

linear ($v_i \neq 0, i = 1, 2, 3$), no matter how skewed the Weyl point is due to the overall constant dispersion $E_0(\mathbf{k})$. In fact, the Weyl nodes carry a quantized Chern flux and can as such only be annihilated by merging with an opposite chirality partner [15]. Furthermore, considering a quasi-two-dimensional slab, one finds that there is a fairly sizable region in which the bandwidth is (much) smaller than the band gap, although to obtain very flat surface bands we need to include also next-nearest-neighbor hopping (as done in Fig. 4). Crucially, this holds true for thin slabs both in the weakly coupled regime studied earlier [30,33,34], as well as when the bulk is in the Weyl semimetal regime.

Thus, one can consider the flatbands of Refs. [30,33,34] vestiges of Weyl semimetal surface bands. While t_{\perp} considered in those works is slightly below the Weyl semimetal regime, our exact solution (2) reveals that this distinction is in fact immaterial in thin slabs as long as only the topological band is concerned.

Projected interactions in the flatband limit.—We now add interactions to a partially filled surface band with $C = N$; for Weyl semimetals with the chemical potential pinned to the Weyl node in the bulk by stoichiometry, this may well be relevant to the low-energy physics of quasi-2D slabs.

The matrix elements of *any* local interaction (provided it is uniform throughout the lattice and does not couple different kagome layers) follows from (2); for a two-body interaction

$$V_{\mathbf{k}_1\mathbf{k}_2\mathbf{k}_3\mathbf{k}_4}^{C=N} = V_{\mathbf{k}_1\mathbf{k}_2\mathbf{k}_3\mathbf{k}_4}^{C=1} \left(\frac{|r(\mathbf{k}_1)|^2 - 1}{|r(\mathbf{k}_1)|^{2N} - 1} \cdots \frac{|r(\mathbf{k}_4)|^2 - 1}{|r(\mathbf{k}_4)|^{2N} - 1} \right)^{1/2} \times \frac{[r^*(\mathbf{k}_1)r^*(\mathbf{k}_2)r(\mathbf{k}_3)r(\mathbf{k}_4)]^N - 1}{r^*(\mathbf{k}_1)r^*(\mathbf{k}_2)r(\mathbf{k}_3)r(\mathbf{k}_4) - 1}, \quad (4)$$

where the band projected interaction Hamiltonian in general can be written as

$$H_{\text{int}} = \sum_{\mathbf{k}_1\mathbf{k}_2\mathbf{k}_3\mathbf{k}_4} V_{\mathbf{k}_1\mathbf{k}_2\mathbf{k}_3\mathbf{k}_4}^{C=N} c_{\mathbf{k}_1}^{\dagger} c_{\mathbf{k}_2}^{\dagger} c_{\mathbf{k}_3} c_{\mathbf{k}_4}, \quad (5)$$

where $c_{\mathbf{k}}^{\dagger}$ ($c_{\mathbf{k}}$) creates (annihilates) an electron in the state $|\psi^{C=N}(\mathbf{k})\rangle$. These expressions generalize straightforwardly to any local $(k+1)$ -body interaction. It is important to note that both the magnitude and the relative phase factors of the matrix elements depend nontrivially on N .

Fractional topological phases.—The flatbands in our model [30] are known to host a series of FCIs in bands with $C > 1$: stable Abelian FCIs of fermions at band filling $\nu = 1/(2C+1)$ and bosons at $\nu = 1/(C+1)$ [33] with non-Abelian phases of bosons at $\nu = k/(C+1)$ using onsite $(k+1)$ -body interactions [34].

Here, we identify a new FCI at filling fraction $\nu = 1/3$, which we propose as a candidate for the first non-Abelian fermionic FCI for $C = 2$, a generalization of the Moore-Read quantum Hall state [35]. This is based on its large and

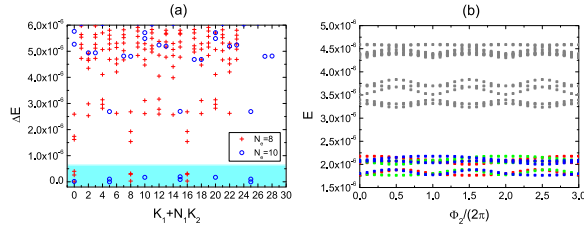


FIG. 5 (color online). Topological degeneracy in the $\mathcal{C} = 2$ bilayer system. (a) The energy spectra of the interaction $H = \sum_{\langle i,j,k \rangle} n_i n_j n_k$ interaction projected to the flatband for $N_e = 8$ and $N_e = 10$ electrons in lattices with $N_1 \times N_2 = (N_e/2) \times 6$ unit cells yielding a filling fraction of $\nu = 1/3$. Each energy level is labeled by the conserved many-body momentum (K_1, K_2) . The shaded area indicates the nine quasidegenerate states. (b) The y -direction spectral flow for eight electrons under twisted boundary conditions $\Psi(\mathbf{r}_j + N_2 \mathbf{a}_2) = \exp(i\Phi_2)\Psi(\mathbf{r}_j)$ of the ground state $\Psi(\mathbf{r}_j)$. The red, green, and blue dots represent the nine quasidegenerate states in different momentum sectors, and the gray dots represent the excited states. The parameters are $t_1 = -1, \lambda_1 = 0.9, t_2 = \lambda_2 = 0$.

robust ninefold topological degeneracy (Fig. 5), its non-trivial entanglement spectra [39], as well as its provenance from a three-body interaction (see [39] for details). We note that, given the flatband is not located at the bottom of the spectrum, this state is indeed naturally suited to fermions at an appropriate density.

Gapless bulk.—Next, we argue that generically, a flat surface band will not be gapped by interactions for thick slabs. This happens because of the—topologically stable—locations on lines in reciprocal space where the states of the band switch the surface at which they are localized. At these points, the inverse penetration depth $\xi^{-1}(\mathbf{k}) = \log(|r(\mathbf{k})|)$ (cf. Fig. 3) vanishes. Matrix elements $V_{\mathbf{k}_1 \mathbf{k}_2 \mathbf{k}_3 \mathbf{k}_4}^{\mathcal{C}=N}$ involving $n_{\{k_i\}}$ momenta on these lines vanish as $(1/\sqrt{N})^{n_{\{k_i\}}}$, reflecting the spatial spread of the wave functions.

This is borne out by our numerics, where the absence of a FCI is indicated by an inhomogeneous electron distribution $n(\mathbf{k})$ in reciprocal space, reminiscent of a Fermi surface (Fig. 6). This is analogous to the compressible states at

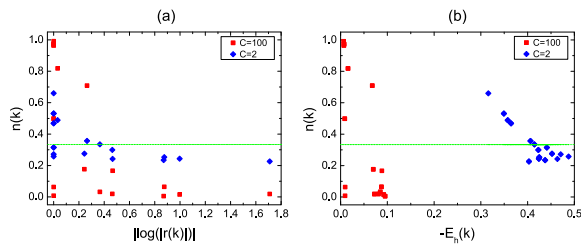


FIG. 6 (color online). Ground state occupation numbers, $n(\mathbf{k})$ plotted against $|\xi[r(\mathbf{k})]|^{-1} = |\log(|r(\mathbf{k})|)|$ (left panel) and $-E_h(\mathbf{k})$ (right panel, cf. Ref. [41]) for Chern numbers $\mathcal{C} = 2$ (blue diamond) and $\mathcal{C} = 100$ (red square) at $\nu = 1/3$. This illustrates a general trend: $n(\mathbf{k})$ is inhomogeneous at large \mathcal{C} , while it can remain comparably constant for small \mathcal{C} (and ν) [39].

high filling fractions in $\mathcal{C} = 1$ bands, where an effective “hole-dispersion,” $E_h(\mathbf{k})$ [39], resulting from a particle-hole transformation, dictates the low-energy physics [41]. In fact, both $\xi^{-1}(\mathbf{k})$ and $E_h(\mathbf{k})$ correlate rather well with $n(\mathbf{k})$ as illustrated for $\nu = 1/3$ with nearest-neighbor repulsion, $H = \sum_{\langle i,j \rangle} n_i n_j$ (Fig. 6, see the Supplemental Material for details and further examples [39]).

Discussion.—In this work, we have unraveled a striking connection between seemingly distinct frontiers of contemporary condensed matter physics by explicitly demonstrating that flatbands with Chern number $\mathcal{C} = N$ appearing on a slab of pyrochlore [30], and known to harbor a rich variety of fractional Chern insulators [33,34], are in fact surface state vestiges of the Fermi arcs of Weyl semimetals [13]. This result has a bearing in the general context of the bulk-boundary correspondence in topological matter: while it has been realized that there can be phase transitions on the boundary while leaving the bulk intact [47,48], we find a striking example of the converse situation with a bulk transition leaving the boundary theory unaffected.

We note that layered structures, albeit with a rather different alternating normal insulator-strong topological insulator setup, have been suggested earlier as a possible platform for Weyl semimetals [14,49]. Weyl semimetals have also been predicted to occur in pyrochlore based bulk materials, in particular in $A_2\text{Ir}_2\text{O}_7$ (A is a rare-earth element) iridates [13], for which the existence of remnant Fermi arc states at certain magnetic domain walls even in the absence of bulk Weyl nodes was recently suggested [17]. Given the experimental advantages with finite pyrochlore slabs grown in the [111] directions [30–32], as compared to other oxide interfaces such as perovskite heterostructures (which may also harbor intriguing flatbands [50,51]), and the generality of our exact solutions for the surface states based solely on locality and lattice geometry, our setup has its distinct advantages even before considering intricate interaction effects.

The exact solutions (1) and (2) provide a generic recipe for “engineering” exotic surface states: coupling Chern insulators with a desirable, e.g., flat, dispersion [52] in a geometrically frustrated manner results in states with the same dispersion but with higher Chern number and added complexity of Fermi arc variety. While we focused on pyrochlore slabs, this procedure generalizes to other frustrated lattices.

We have also explored the effect of interactions in these bands and identified new fractionalized topological phases as well as generic gapless states as $\mathcal{C} \rightarrow \infty$. Our work establishes that the combined fractionalization and topological surface localization of the interacting states found here, and in Refs. [33,34], are impossible in strictly two-dimensional (isotropic) models just as Fermi arcs cannot exist in purely two-dimensional band materials. This feature distinguishes the pyrochlore based FCIs from other $\mathcal{C} > 1$ generalizations of multilayer quantum Hall states [53–61].

The present Letter invites a number of interesting questions regarding the interplay between fractionalization, surface localization, and translation symmetry. In this context, it would be particularly interesting to investigate the effects of lattice dislocations [53,62].

We thank J. Behrmann and A. Läuchli for related collaborations. E.J.B. is grateful to P. Brouwer, T. Ojanen, and B. Sbierski for numerous discussions on Weyl semimetals. E.J.B. and M.T. are supported by DFG's Emmy Noether Program (No. BE 5233/1-1). Z. L. is supported by the Department of Energy, Office of Basic Energy Sciences, through Grant No. DE-SC0002140. M. U. is supported by Grants-in-Aid for Scientific Research (No. 24340076, No. 26400339, and No. 24740221). This work was in part supported by the Helmholtz VI "New States of Matter and Their Excitations."

-
- [1] C. L. Kane and E. J. Mele, *Phys. Rev. Lett.* **95**, 226801 (2005).
- [2] B. A. Bernevig, T-L Hughes, and S.-C. Zhang, *Science* **314**, 1757 (2006).
- [3] J. E. Moore and L. Balents, *Phys. Rev. B* **75**, 121306 (2007).
- [4] L. Fu, C. L. Kane, and E. J. Mele, *Phys. Rev. Lett.* **98**, 106803 (2007).
- [5] R. Roy, *Phys. Rev. B* **79**, 195322 (2009).
- [6] M. König, S. Wiedmann, C. Brüne, A. Roth, H. Buhmann, L. W. Molenkamp, X.-L. Qi, and S.-C. Zhang, *Science* **318**, 766 (2007).
- [7] D. Hsieh, D. Qian, L. Wray, Y. Xia, Y. S. Hor, R. J. Cava, and M. Z. Hasan, *Nature (London)* **452**, 970 (2008).
- [8] M. Z. Hasan and C. L. Kane, *Rev. Mod. Phys.* **82**, 3045 (2010).
- [9] X.-L. Qi and S.-C. Zhang, *Rev. Mod. Phys.* **83**, 1057 (2011).
- [10] B. A. Bernevig and T. L. Hughes, *Topological Insulators and Topological Superconductors* (Princeton University Press, Princeton, NJ, 2013).
- [11] G. E. Volovik, *The Universe in a Helium Droplet* (Clarendon, Oxford, 2003).
- [12] S. Murakami, *New J. Phys.* **9**, 356 (2007).
- [13] X. Wan, A. M. Turner, A. Vishwanath, and S. Y. Savrasov, *Phys. Rev. B* **83**, 205101 (2011).
- [14] A. A. Burkov and L. Balents, *Phys. Rev. Lett.* **107**, 127205 (2011).
- [15] For reviews, see A. M. Turner and A. Vishwanath, arXiv: 1301.0330; P. Hosur and X. Qi, *C.R. Phys.* **14**, 857 (2013).
- [16] T. Ojanen, *Phys. Rev. B* **87**, 245112 (2013).
- [17] Y. Yamaji and M. Imada, *Phys. Rev. X* **4**, 021035 (2014).
- [18] M. Sitte, A. Rosch, and L. Fritz, *Phys. Rev. B* **88**, 205107 (2013).
- [19] C. Wang, A. C. Potter, and T. Senthil, *Phys. Rev. B* **88**, 115137 (2013).
- [20] M. A. Metlitski, C. L. Kane, and M. P. A. Fisher, arXiv: 1306.3286.
- [21] P. Bonderson, C. Nayak, and X.-L. Qi, *J. Stat. Mech.* (2013) P09016.
- [22] X. Chen, L. Fidkowski, and A. Vishwanath, *Phys. Rev. B* **89**, 165132 (2014).
- [23] E. J. Bergholtz and Z. Liu, *Int. J. Mod. Phys. B* **27**, 1330017 (2013).
- [24] S. A. Parameswaran, R. Roy, and S. L. Sondhi, *C.R. Phys.* **14**, 816 (2013).
- [25] J. Mannhart and D. G. Schlom, *Science* **327**, 1607 (2010).
- [26] M. Neupane, S.-Y. Xu, R. Sankar, N. Alidoust, G. Bian, C. Liu, I. Belopolski, T.-R. Chang, H.-T. Jeng, H. Lin, A. Bansil, F. Chou, and M. Z. Hasan, *Nat. Commun.* **5**, 3786 (2014).
- [27] S. Borisenko, Q. Gibson, D. Evtushinsky, V. Zabolotnyy, B. Büchner, and R. J. Cava, *Phys. Rev. Lett.* **113**, 027603 (2014).
- [28] Z. K. Liu, B. Zhou, Y. Zhang, Z. J. Wang, H. M. Weng, D. Prabhakaran, S.-K. Mo, Z. X. Shen, Z. Fang, X. Dai, Z. Hussain, and Y. L. Chen, *Science* **343**, 864 (2014).
- [29] H.-J. Kim, K.-S. Kim, J.-F. Wang, M. Sasaki, N. Satoh, A. Ohnishi, M. Kitaura, M. Yang, and L. Li, *Phys. Rev. Lett.* **111**, 246603 (2013).
- [30] M. Trescher and E. J. Bergholtz, *Phys. Rev. B* **86**, 241111 (R) (2012).
- [31] X. Hu, A. Rüegg, and G. A. Fiete, *Phys. Rev. B* **86**, 235141 (2012).
- [32] B.-J. Yang and N. Nagaosa, *Phys. Rev. Lett.* **112**, 246402 (2014).
- [33] Z. Liu, E. J. Bergholtz, H. Fan, and A. M. Läuchli, *Phys. Rev. Lett.* **109**, 186805 (2012).
- [34] A. Sterdyniak, C. Repellin, B. Andrei Bernevig, and N. Regnault, *Phys. Rev. B* **87**, 205137 (2013).
- [35] G. Moore and N. Read, *Nucl. Phys.* **B360**, 362 (1991).
- [36] F. D. M. Haldane, *Phys. Rev. Lett.* **61**, 2015 (1988).
- [37] E. Tang, J.-W. Mei, and X.-G. Wen, *Phys. Rev. Lett.* **106**, 236802 (2011).
- [38] Z.-X. Liu, J.-W. Mei, P. Ye, and X.-G. Wen, arXiv: 1408.1676.
- [39] See Supplemental Material at <http://link.aps.org/supplemental/10.1103/PhysRevLett.114.016806>, which includes Refs. [30,40–46], for more details.
- [40] N. R. Cooper, N. K. Wilkin, and J. M. F. Gunn, *Phys. Rev. Lett.* **87**, 120405 (2001).
- [41] A. M. Läuchli, Z. Liu, E. J. Bergholtz, and R. Moessner, *Phys. Rev. Lett.* **111**, 126802 (2013).
- [42] N. Regnault and B. A. Bernevig, *Phys. Rev. X* **1**, 021014 (2011).
- [43] A. Sterdyniak, N. Regnault, and B. A. Bernevig, *Phys. Rev. Lett.* **106**, 100405 (2011).
- [44] M. Greiter, X.-G. Wen, and F. Wilczek, *Phys. Rev. Lett.* **66**, 3205 (1991).
- [45] B. A. Bernevig and N. Regnault, *Phys. Rev. B* **85**, 075128 (2012).
- [46] Y.-F. Wang, H. Yao, Z.-C. Gu, C.-D. Gong, and D. N. Sheng, *Phys. Rev. Lett.* **108**, 126805 (2012).
- [47] J. Cano, M. Cheng, M. Mulligan, C. Nayak, E. Plamadeala, and J. Yard, *Phys. Rev. B* **89**, 115116 (2014).
- [48] A. Chandran, V. Khemani, and S. L. Sondhi, *Phys. Rev. Lett.* **113**, 060501 (2014).
- [49] A. A. Burkov, M. D. Hook, and L. Balents, *Phys. Rev. B* **84**, 235126 (2011).
- [50] D. Xiao, W. Zhu, Y. Ran, N. Nagaosa, and S. Okamoto, *Nat. Commun.* **2**, 596 (2011).
- [51] F. Wang and Y. Ran, *Phys. Rev. B* **84**, 241103(R) (2011).

- [52] E. Kapit and E. Mueller, *Phys. Rev. Lett.* **105**, 215303 (2010).
- [53] M. Barkeshli and X.-L. Qi, *Phys. Rev. X* **2**, 031013 (2012).
- [54] Y.-F. Wang, H. Yao, C.-D. Gong, and D. N. Sheng, *Phys. Rev. B* **86**, 201101(R) (2012).
- [55] S. Yang, Z.-C. Gu, K. Sun, and S. Das Sarma, *Phys. Rev. B* **86**, 241112(R) (2012).
- [56] L. Hormozi, G. Moller, and S. H. Simon, *Phys. Rev. Lett.* **108**, 256809 (2012).
- [57] A. G. Grushin, T. Neupert, C. Chamon, and C. Mudry, *Phys. Rev. B* **86**, 205125 (2012).
- [58] Y.-L. Wu, N. Regnault, and B. A. Bernevig, *Phys. Rev. Lett.* **110**, 106802 (2013).
- [59] D. Wang, Z. Liu, J. Cao, and H. Fan, *Phys. Rev. Lett.* **111**, 186804 (2013).
- [60] Y.-H. Wu, J. K. Jain, and K. Sun, [arXiv:1309.1698](https://arxiv.org/abs/1309.1698).
- [61] M. Udagawa and E. J. Bergholtz, *J. Stat. Mech.* (2014) P10012.
- [62] Y. Ran, Y. Zhang, and A. Vishwanath, *Nat. Phys.* **5**, 298 (2009).